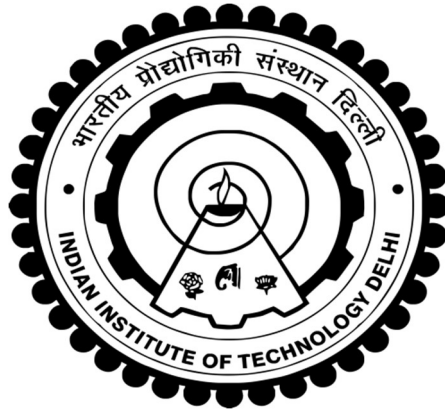


**DESIGN AND DEVELOPMENT OF HIGH EFFICIENCY THREE
PHASE INDUCTION MOTORS FOR SOLAR WATER PUMPING
AND OTHER APPLICATIONS**

KHUSRO KHAN



**DEPARTMENT OF ELECTRICAL ENGINEERING
INDIAN INSTITUTE OF TECHNOLOGY DELHI
MARCH 2022**

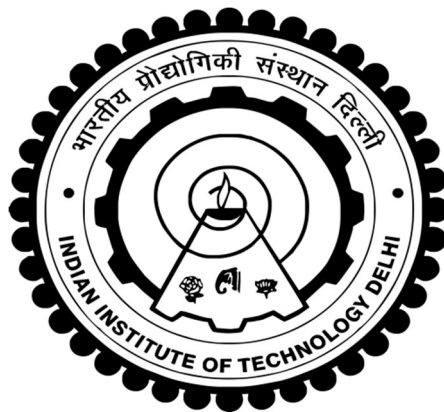
©Indian Institute of Technology Delhi (IITD), New Delhi, 2022

**DESIGN AND DEVELOPMENT OF HIGH EFFICIENCY THREE
PHASE INDUCTION MOTORS FOR SOLAR WATER PUMPING
AND OTHER APPLICATIONS**

by

KHUSRO KHAN
Electrical Engineering Department

Submitted
in fulfillment of the requirements of the degree of Doctor of Philosophy
to the



INDIAN INSTITUTE OF TECHNOLOGY DELHI
MARCH 2022

CERTIFICATE

It is certified that the thesis entitled “**Design and Development of High Efficiency Three Phase Induction Motors for Solar Water Pumping and Other Applications,**” being submitted by **Mr. Khusro Khan** for award of the degree of **Doctor of Philosophy** in the Department of Electrical Engineering, Indian Institute of Technology Delhi, is a record of the student work carried out by him under my supervision and guidance. The matter embodied in this thesis has not been submitted for award of any other degree or diploma.

Dated: March 10, 2022

(Prof. Bhim Singh)
Electrical Engineering Department
Indian Institute of Technology Delhi
Hauz Khas, New Delhi-110016, India

ACKNOWLEDGEMENTS

I wish to express my deepest gratitude and indebtedness to **Prof. Bhim Singh** for providing me guidance and constant supervision to carry out the Ph.D. work. Determination, dedication, innovativeness, resourcefulness and discipline of **Prof. Bhim Singh** have been the inspiration for me to complete this work. I truly appreciate and value his esteemed guidance and encouragement from the beginning to the end of this thesis. His continuous monitoring and commitments to excellence have always motivated me to improve my work and use the best of my capabilities. His guidance helped me in all the time of research and writing of this thesis. I could not have imagined having a better advisor and mentor for my Ph.D. study.

My sincere thanks and deep gratitude are to **Prof. Sukumar Mishra, Prof. G. Bhuvaneswari,** and **Dr. Ashu Verma**, all SRC members for their valuable guidance and consistent support during my research work.

I wish to convey my sincere thanks to **Prof. Bhim Singh, Prof. B. P. Singh, Prof. G. Bhuvaneswari** and the late **Prof. K. R. Rajagopal** for their valuable inputs during my course work, which made the foundation for my research work. I am grateful to IIT Delhi for providing me the research facilities. I would wish to express my sincere gratitude to **Prof. Bhim Singh, Prof. G. Bhuvaneswari** and the late **Prof. K. R. Rajagopal**, as Prof. in-charge of PG Machines Lab, for providing me immense facilities to carry out experimental work.

I would like to use this opportunity to thank Dr. Aniket Anand, Dr. Chinmay Jain, Dr. Rajan Kumar, Dr. Ikhlq Hussain, Dr. Shailendra Dwivedi and Dr. Anjaneer Kumar Mishra, who have helped me in deciding my research goal and helped me sincerely in the initial phase of my journey in Ph.D. My sincere thanks are due to Dr. Saurabh Shukla for helping me throughout my research journey. It would be incomplete without thanking Dr. Shadab Murshid, without whose support it

would have been very difficult to complete this research work. I would like to thank Mr. Vineet. P. Chandran, Dr. Piyush Kant, Dr. Deepu Vijay Menon and Dr. Priyank Shah for their constant support and motivation for performance excellence. My sincere thanks go to Miss Farheen Chisti, Mr Kashif, Mr. Aryadeep Sengupta, Ms. Rashmi Rai, Mr. Syed Bilal Ahmed, and all PG Machines laboratory group for their valuable support.

I am grateful to **Mr. Dheeraj Prasad**, Plant Head, Manufacturing facility for three phase induction motors, ABB India ltd. Faridabad, for having given me an opportunity to pursue my research at IIT Delhi, by extending the facilities to carry out my research work at ABB India Ltd., Faridabad. His consistent encouragement and valuable guidance have been instrumental in achieving the targets, envisaged in my research work.

I would like to convey my unbounded love to my grandfather late **Mr. Abdul Kareem Khan** and my grandmother **Mrs. Hamidun Nisa Begum** for showering their blessings on me. A great deal of effort, endurance, encouragement and blessings of my parents **Mrs. Azizun Nisa Begum** and late **Mr. Abdul Qadeer Khan** are worthy to be remembered. Moreover, I would like to thank my brothers **Mr. Abdul Hafeez Khan** and **Mr. Imran Khan**, and other family members for giving me the inner strength and wholehearted support. Their trust in my capabilities had been a key factor to all my achievements. I would like to thank my wife **Mrs. Iram Hasan Khan** for the patience all throughout the research work. The patience, encouragement and firm support of my wife earns deepest love and appreciation, without her support this work could not be completed. The patience of my kids **Khubair**, **Kaleem** and **Fatima** has given me a consistent support to perform under adverse situations.

At last, I am beholden to almighty for their blessings to help me to raise my academic level to this stage. I pray for their benediction in my future endeavors. Their blessings may be showered on me for strength, wisdom, and determination to achieve in future.

Date: 10.03.2022

Khusro Khan

ABSTRACT

This thesis deals with an efficiency optimization method of the induction motor (IM) through the variation of the different design parameters. To achieve this goal, the flux in the airgap, in the yoke, in the teeth is modified according to an optimal flux table computed off-line for all possible operating points. The design of this motor is achieved through a combined approach of design of experiments (DOE) with one of the optimization algorithms. The design and parameter constraints are function of the geometry of the motor. The proposed optimization method is implemented, and optimized motor then tested for the field-oriented control, to show the genericity of the proposed approach. The validation is carried on an experimental test bench for six induction motors of different power ratings. The results obtained show the reduction of the losses in the motor, thus an improvement of the overall efficiency while preserving a satisfactory dynamic behavior. Consequently, the optimization of the energy efficiency is validated for the six developed motors for different low power applications i.e., fan application, pump application and electric vehicle application. In addition to the validation of the simulation results, the proposed approach is compared to existing conventional standard motors to assess its improvement.

The performance of the induction motor is changed by changing its core length, shape of stator slots, shape of rotor slots or the diameter of the core, material of the stampings, material of the casting i.e., aluminum or copper in the rotor, skew angle, and air gap length. In the variable frequency drive, the first two requirement of high starting torque and low starting current are taken care by voltage source inverter (VSI). Therefore, this work focuses on the efficiency improvement of the motor. In this case, the design and construction of induction motors are based on standard

motors with standardized frame sizes and dimensions, however, with modifications for converter operation.

The utilization of solar photovoltaic (PV) energy in water pumping is conservative particularly in isolated regions where the transmission of power is either impractical or exorbitant. In this research work, various topologies for solar PV array fed water pumping are developed using an induction motor drive. A high efficiency induction motor substantially reduces the size of PV array and hence its installation cost. Moreover, its high-power factor results in a reduced capacity of the used voltage source inverter (VSI). Therefore, in this work, mechanical sensorless control of an induction motor drive is investigated with fast speed control and better stability. The motor flux is optimized, and the total losses are minimized in partial loading condition. The system is made simplified and cost-effective by reducing the number of voltage and current sensors and all parameters are estimated through the sensed DC link voltage and DC link current. The system possesses a maximum power point tracking (MPPT) of the PV array by introducing a DC-DC boost converter between the PV array and a VSI, feeding the motor. The work is extended towards an elimination of a DC-DC converter and a single stage PV array fed induction motor drive is also investigated for water pumping.

A promising case of interruption in the water pumping due to the intermittency of PV power generation is resolved by using a single-phase utility grid as an external power backup. A grid interacted PV array and its control are demonstrated to get a reliable and fully utilized water pumping with an induction motor such that the pumping is not affected by an intermittency of solar PV array generation. The power is drawn from the grid in case the PV array is unable to meet the required power demand. Both unidirectional and bidirectional power flow controls are implemented for a grid interfaced PV array fed induction motor driven water pump. The

bidirectional power flow control-based topology offers an additional merit of feeding power to the utility grid by the installed PV array, in case the water pumping is not required. This practice leads to a full utilization of installed resources. Moreover, it emerges as a source of earning by sale of electricity to the utility. The maximum power point (MPP) operation of a PV array, and power quality (PQ) standards such as power factor and total harmonic distortion (THD) of the grid current as per IEEE-519 standard, are met by this system.

A single-phase grid fed fan type load profile system operated by a mechanical sensorless induction motor drive suitable to work in complete speed range is developed and a unidirectional power flow control for the same is developed and realized through a power factor corrected (PFC) boost converter. This research work also aims on the power factor correction in the induction motor drive for fan application with the speed control. A power factor corrected (PFC) boost converter is utilized for the development of the system. A full speed range of a fan with enhanced power quality during normal and abnormal grid voltage conditions is achieved by using this system. The system is simulated and analyzed under variable speed and load conditions, during both the normal and weak grid, for a fan type load profile.

Hike in price due to limited and rapidly exhausting oil deposition have forced the automobile industry to find economically feasible alternative sources of energy to drive them forward. In this context, the use of a battery operated EV's becomes poignantly significant all over the world. Not much effort has been taken to counter this crisis, especially in developing countries such as India due to the non-availability of technology and expert knowledge in this domain. This research work elaborates the design and development of EV drive motors using die-cast copper rotor technology and regulating it with an economic and efficient drive controller.

All the proposed configurations are modeled and simulated using MATLAB/Simulink platform to demonstrate their performance during starting, dynamics and steady state conditions. Simulated results are verified through test results obtained from hardware implementation using a developed prototype in the laboratory. The applicability and commercial potential of proposed systems are justified by their in-depth analysis based on efficiency, cost, simplicity, and performance.

सारांश

यह थीसिस विभिन्न डिजाइन मापदंडों की भिन्नता के माध्यम से प्रेरण मोटर (आईएम) की दक्षता अनुकूलन विधि से संबंधित है। इस लक्ष्य को प्राप्त करने के लिए, एयरगैप में प्रवाह, योक में, दांतों में सभी संभावित ऑपरेटिंग बिंदुओं के लिए ऑफ-लाइन गणना की गई इष्टतम प्रवाह तालिका के अनुसार संशोधित किया जाता है। इस मोटर का डिजाइन अनुकूलन एल्गोरिदम में से एक के साथ प्रयोगों (डीओई) के डिजाइन के संयुक्त दृष्टिकोण के माध्यम से प्राप्त किया जाता है। डिजाइन और पैरामीटर बाधाएं मोटर की ज्यामिति का कार्य हैं। प्रस्तावित अनुकूलन विधि लागू की जाती है, और प्रस्तावित दृष्टिकोण की सामान्यता दिखाने के लिए क्षेत्र-उन्मुख नियंत्रण के लिए अनुकूलित मोटर का परीक्षण किया जाता है। सत्यापन विभिन्न पावर रेटिंग के छह प्रेरण मोटर्स के लिए एक प्रयोगात्मक परीक्षण बेंच पर किया जाता है। प्राप्त परिणाम मोटर में नुकसान में कमी दिखाते हैं, इस प्रकार संतोषजनक गतिशील व्यवहार को संरक्षित करते हुए समग्र दक्षता में सुधार होता है। नतीजतन, ऊर्जा दक्षता का अनुकूलन विभिन्न कम बिजली अनुप्रयोगों यानी, प्रशंसक अनुप्रयोग, पंप अनुप्रयोग और इलेक्ट्रिक वाहन अनुप्रयोग के लिए छह विकसित मोटर्स के लिए मान्य है। सिमुलेशन परिणामों के सत्यापन के अलावा, प्रस्तावित दृष्टिकोण की तुलना मौजूदा पारंपरिक मानक मोटर्स से की जाती है ताकि इसके सुधार का आकलन किया जा सके।

प्रेरण मोटर का प्रदर्शन इसकी कोर लंबाई, स्टेटर स्लॉट के आकार, रोटर स्लॉट के आकार या कोर के व्यास, मुद्रांकन की सामग्री, कास्टिंग की सामग्री यानी रोटर में एल्यूमीनियम या तांबा, तिरछा कोण और वायु अंतराल लंबाई को बदलकर बदल दिया जाता है। चर आवृत्ति ड्राइव में, उच्च शुरुआती टोक और कम शुरुआती वर्तमान की पहली दो आवश्यकताओं को वोल्टेज स्रोत इन्वर्टर (वीएसआई) द्वारा ध्यान रखा जाता है। इसलिए, यह काम मोटर की दक्षता में सुधार पर केंद्रित है। इस मामले में, प्रेरण मोटर्स का डिजाइन और

निर्माण मानकीकृत फ्रेम आकार और आयामों के साथ मानक मोटर्स पर आधारित है, हालांकि, कनवर्टर ऑपरेशन के लिए संशोधनों के साथ।

पानी की पंपिंग में सौर फोटोवोल्टिक (पीवी) ऊर्जा का उपयोग विशेष रूप से अलग-थलग क्षेत्रों में रूढ़िवादी है जहां बिजली का संचरण या तो अव्यावहारिक या अत्यधिक है। इस शोध कार्य में, सौर पीवी सरणी खिलाया पानी पंपिंग के लिए विभिन्न टोपोलॉजी एक प्रेरण मोटर ड्राइव का उपयोग करके विकसित की जाती हैं एक उच्च दक्षता प्रेरण मोटर पीवी सरणी के आकार को काफी कम कर देता है और इसलिए इसकी स्थापना लागत। इसके अलावा, इसके उच्च शक्ति कारक के परिणामस्वरूप उपयोग किए गए वोल्टेज स्रोत इन्वर्टर (वीएसआई) की क्षमता कम हो जाती है। इसलिए, इस काम में, एक प्रेरण मोटर ड्राइव के यांत्रिक सेंसररहित नियंत्रण की तेज गति नियंत्रण और बेहतर स्थिरता के साथ जांच की जाती है। मोटर प्रवाह अनुकूलित है, और आंशिक लोडिंग स्थिति में कुल नुकसान को कम किया जाता है। वोल्टेज और वर्तमान सेंसर की संख्या को कम करके सिस्टम को सरलीकृत और लागत प्रभावी बनाया जाता है और सभी मापदंडों का अनुमान डीसी लिंक वोल्टेज और डीसी लिंक वर्तमान के माध्यम से लगाया जाता है। सिस्टम में पीवी सरणी और वीएसआई के बीच डीसी-डीसी बूस्ट कनवर्टर पेश करके पीवी सरणी का अधिकतम पावर पॉइंट ट्रैकिंग (एमपीपीटी) है, जो मोटर को खिलाता है। काम को डीसी-डीसी कनवर्टर के उन्मूलन की दिशा में बढ़ाया जाता है और पानी पंपिंग के लिए एक एकल चरण पीवी सरणी खिलाया प्रेरण मोटर ड्राइव की भी जांच की जाती है।

पीवी बिजली उत्पादन की आंतरायिकता के कारण पानी पंपिंग में रुकावट का एक आशाजनक मामला बाहरी बिजली बैकअप के रूप में एकल-चरण उपयोगिता ग्रिड का उपयोग करके हल किया जाता है। एक ग्रिड ने पीवी सरणी और इसके नियंत्रण को एक प्रेरण मोटर के साथ एक विश्वसनीय और पूरी तरह

से उपयोग किए जाने वाले पानी के पंपिंग को प्राप्त करने के लिए प्रदर्शित किया जाता है जैसे कि पंपिंग सौर पीवी सरणी पीढ़ी की आंतरायिकता से प्रभावित नहीं होती है। यदि पीवी सरणी आवश्यक बिजली की मांग को पूरा करने में असमर्थ है तो बिजली ग्रिड से खींची जाती है। यूनिडायरेक्शनल और द्विदिश बिजली प्रवाह नियंत्रण दोनों ग्रिड इंटरफेस पीवी सरणी खिलाया प्रेरण मोटर संचालित पानी पंप के लिए लागू किए जाते हैं। द्विदिश बिजली प्रवाह नियंत्रण-आधारित टोपोलॉजी स्थापित पीवी सरणी द्वारा उपयोगिता ग्रिड को बिजली खिलाने की एक अतिरिक्त योग्यता प्रदान करती है, यदि पानी पंपिंग की आवश्यकता नहीं है। यह अभ्यास स्थापित संसाधनों के पूर्ण उपयोग की ओर जाता है। इसके अलावा, यह उपयोगिता को बिजली की बिक्री करके कमाई के स्रोत के रूप में उभरता है। आईईईई -519 मानक के अनुसार ग्रिड वर्तमान के पीवी सरणी के अधिकतम पावर पॉइंट (एमपीपी) ऑपरेशन, और पावर क्वालिटी (पीक्यू) मानकों जैसे पावर फैक्टर और कुल हार्मोनिक विरूपण (टीएचडी) को इस प्रणाली द्वारा पूरा किया जाता है।

पूर्ण गति सीमा में काम करने के लिए उपयुक्त एक यांत्रिक सेंसरलेस प्रेरण मोटर ड्राइव द्वारा संचालित एक एकल-चरण ग्रिड खिलाया प्रशंसक प्रकार लोड प्रोफाइल सिस्टम विकसित किया जाता है और उसी के लिए एक यूनिडायरेक्शनल पावर फ्लो कंट्रोल विकसित किया जाता है और पावर फैक्टर सही (पीएफसी) बूस्ट कनवर्टर के माध्यम से महसूस किया जाता है। इस शोध कार्य का उद्देश्य गति नियंत्रण के साथ प्रशंसक अनुप्रयोग के लिए प्रेरण मोटर ड्राइव में पावर फैक्टर सुधार भी है। सिस्टम के विकास के लिए पावर फैक्टर सही (पीएफसी) बूस्ट कनवर्टर का उपयोग किया जाता है। सामान्य और असामान्य ग्रिड वोल्टेज स्थितियों के दौरान बढ़ी हुई बिजली की गुणवत्ता के साथ एक प्रशंसक की एक पूर्ण गति सीमा इस प्रणाली का उपयोग करके प्राप्त की जाती है। सिस्टम को एक प्रशंसक प्रकार लोड प्रोफाइल के लिए सामान्य और कमजोर ग्रिड दोनों के दौरान चर गति और लोड स्थितियों के तहत अनुकरण और विश्लेषण किया जाता है।

सीमित और तेजी से व्यय तेल जमाव के कारण कीमतों में वृद्धि ने ऑटोमोबाइल उद्योग को उन्हें आगे बढ़ाने के लिए ऊर्जा के आर्थिक रूप से व्यवहार्य वैकल्पिक स्रोतों को खोजने के लिए मजबूर किया है। इस संदर्भ में, बैटरी संचालित ईवी का उपयोग दुनिया भर में मार्मिक रूप से महत्वपूर्ण हो जाता है। इस संदर्भ में, बैटरी संचालित ईवी का उपयोग दुनिया भर में मार्मिक रूप से महत्वपूर्ण हो जाता है। इस संकट का मुकाबला करने के लिए बहुत अधिक प्रयास नहीं किए गए हैं, खासकर भारत जैसे विकासशील देशों में इस क्षेत्र में प्रौद्योगिकी और विशेषज्ञ ज्ञान की अनुपलब्धता के कारण। यह शोध कार्य ड्राई-कास्ट कॉपर रोटार तकनीक का उपयोग करके ईवी ड्राइव मोटर्स के डिजाइन और विकास को विस्तृत करता है और इसे आर्थिक और कुशल ड्राइव नियंत्रक के साथ विनियमित करता है।

सभी प्रस्तावित कॉन्फ़िगरेशन को शुरूआती, गतिशीलता और स्थिर स्थिति स्थितियों के दौरान उनके प्रदर्शन को प्रदर्शित करने के लिए मैटलैब / सिमुलिक प्लेटफ़ॉर्म का उपयोग करके मॉडलिंग और सिमुलेटेड किया गया है। प्रयोगशाला में एक विकसित प्रोटोटाइप का उपयोग करके हार्डवेयर कार्यान्वयन से प्राप्त परीक्षण परिणामों के माध्यम से नकली परिणामों को सत्यापित किया जाता है। प्रस्तावित प्रणालियों की प्रयोज्यता और वाणिज्यिक क्षमता दक्षता, लागत, सादगी और प्रदर्शन के आधार पर उनके गहन विश्लेषण द्वारा उचित है।

TABLE OF CONTENTS

Certificate	i
Acknowledgements	ii
Abstract	v
Table of Contents	xiii
List of Figures	xxii
List of Tables	xxix
List of Abbreviations	xxxiv
List of Symbols	xxxvi
CHAPTER I INTRODUCTION	1-18
1.1 General	1
1.2 State of Art	7
1.3 Objectives and Scope of Work	11
1.4 Outline of Chapters	14
CHAPTER II LITERATURE REVIEW	19-41
2.1 General	19
2.2 History and Development of Induction Motors	20
2.3 History and Development of PV Technology	24
2.4 Standards, Testing and Quality Certification for Three Phase Induction Motor	26
2.5 Standards, Testing and Quality Certification for Solar PV System	26
2.6 Literature Survey	27
2.6.1 Efficiency Improvement Measures in Induction Motors	27
2.6.2 Review of Optimal Design of Induction Motors	28
2.6.3 Review of Classical Methods of Optimization for Efficiency Optimal Design of Induction Motor	28
2.6.4 Review of Optimization Algorithms in Energy Efficient Induction Motors	30
2.6.5 Review of Advantages of Copper Bar Rotor against Aluminium Bar Rotor	30
2.6.6 Review of Solar PV Fed Water Pumping Systems	31
2.6.6.1 Solar PV Fed DC Motor Driven Water Pumping	32
2.6.6.2 Solar PV Fed BLDC Motor Driven Water Pumping	32
2.6.6.3 Solar PV Fed Induction Motor Driven Water Pumping	33
2.6.6.4 Solar PV Fed PMSM Driven Water Pumping	34
2.6.6.5 Solar PV Fed SRM Driven Water Pumping	35
2.6.6.6 Solar PV Fed SyRM Driven Water Pumping	36
2.6.7 Review of Mechanical Sensorless Techniques for Solar PV fed Induction Motor Drive for Water Pumping	36
2.6.8 Review of Power Factor Correction of PV fed High Efficiency Induction Motor Drives	38

2.7	Identified Research Areas	39
2.8	Conclusions	40
CHAPTER III DEVELOPMENT OF HIGH EFFICIENCY THREE PHASE SQUIRREL CAGE INDUCTION MOTORS		42-133
3.1	General	42
3.2	Conventional Efficiency Improvement Measures in Electric Drive Systems	43
3.3	Design Approach for High Efficiency Motor for Solar Water Pumping and Other Applications	45
3.3.1	Performance Parameters of Induction Motor for Solar PV fed Water Pumping and Other Applications	53
3.3.2	Parametric Analysis of Induction Motor for Solar PV fed Water Pumping and Other Applications	56
3.3.3	Design of High Efficiency Induction Motor for Solar PV fed Water Pumping and other Applications	63
3.3.4	Design Optimization of Induction Motor	72
3.3.5	Finite Element Analysis of High Efficiency Induction Motor for Solar PV fed Water Pumping and Other Applications	79
3.4	Test Set Up Hardware of High Efficiency Induction Motor for Solar PV fed Water Pumping and Other Applications	85
3.4.1	Configuration of Motor Performance Test Setup	85
3.4.2	Testing and Measurement of High Efficiency Induction Motors for Solar PV fed Water Pumping and Other Applications	86
3.5	Results and Discussion	125
3.5.1	Comparison of Simulated Performance of 0.75 kW ,1.5 kW and 2.2kW High Efficiency Induction Motor for Solar PV fed Water Pumping and Other Applications with Conventional Motor	125
3.5.1.1	A Comparison of Simulated Efficiency of 0.75 kW ,1.5 kW and 2.2kW High Efficiency Induction Motor with Conventional Motor	126
3.5.1.2	A Comparison of Simulated Starting Performance of 0.75 kW, 1.5kW and 2.2kW High Efficiency Induction Motor with Conventional Motor	128
3.5.2	Comparison of Test Results Obtained from 0.75 kW ,1.5 kW and 2.2kW High Efficiency Induction Motor for Solar PV fed Water Pumping and Other Applications with Conventional Motor	129
3.5.2.1	Efficiency Comparison of 0.75 kW ,1.5 kW and 2.2kW High Efficiency Induction Motor with Conventional Motor from Test Results	130
3.5.2.2	Speed-Torque Characteristics Comparison of 0.75 kW ,1.5 kW and 2.2kW High Efficiency Induction Motor with Conventional Motor from Test Results	132

3.6	Conclusions	132
CHAPTER IV	STANDALONE SOLAR PV FED MECHANICAL SENSORLESS HIGH EFFICIENCY INDUCTION MOTOR DRIVE FOR WATER PUMPING	134-182
4.1	General	134
4.2	Configuration of Standalone Solar PV Fed Mechanical Sensorless High Efficiency Induction Motor Drive for Water Pumping	135
4.2.1	Configuration of Solar PV Fed Mechanical Sensorless High Efficiency Induction Motor Drive for Water Pumping with Boost Converter	136
4.2.2	Configuration of Single Stage Solar PV Fed Mechanical Sensorless High Efficiency Induction Motor Drive for Water Pumping	136
4.3	Design of Standalone Solar PV Fed Mechanical Sensorless High Efficiency Induction Motor Drive for Water Pumping	138
4.3.1	Design of Solar PV Fed Mechanical Sensorless High Efficiency Induction Motor Drive for Water Pumping Using Boost Converter	138
4.3.1.1	Design and Selection of Solar PV Array	139
4.3.1.2	Design of Boost Converter	139
4.3.1.3	Design of DC Link Capacitor	140
4.3.1.4	Selection of DC Link Voltage	140
4.3.1.5	Design of VSI	141
4.3.1.6	Design of Water Pump	142
4.3.2	Design of Single Stage Solar PV Fed Mechanical Sensorless Induction Motor Drive for Water Pumping Using Boost Converter	143
4.3.2.1	Design and Selection of Solar PV Array	144
4.3.2.2	Design of DC Link Capacitor	144
4.3.2.3	Selection of DC Link Voltage	145
4.3.2.4	Design of VSI	145
4.3.2.5	Design of Water Pump	145
4.4	Speed Estimation of High Efficiency Induction Motor Drive	146
4.5	Control of Solar PV Fed High Efficiency Induction Motor Drive for Water Pumping	148
4.5.1	Control of Solar PV Fed High Efficiency Induction Motor Drive for Water Pumping Using Boost Converter	148
4.5.1.1	MPPT Control of Solar PV Array	148
4.5.1.2	Field-Oriented Control of Induction Motor Drive	151
4.5.2	Control of Single Stage Solar PV Fed High Efficiency Induction Motor Drive for Water Pumping	154
4.5.2.1	MPPT Control of Solar PV Array	154
4.5.2.2	Field-Oriented Control of Induction Motor Drive	154

4.6	MATLAB Based Modeling and Simulation of PV Array Fed High Efficiency Induction Motor Drive for Water Pumping	157
4.7	Hardware Implementation of PV Array Fed High Efficiency Induction Motor Drive for Water Pumping	160
4.7.1	Development of Signal Conditioning Circuit for Voltage Sensors	160
4.7.2	Development of Signal Conditioning Circuit for Current Sensors	161
4.7.3	Development of Isolation and Amplification Circuit for Gate Drivers	1623
4.7.4	Execution of Control Algorithm on DSP-dSPACE 1202	163
4.8	Results and Discussion	165
4.8.1	Simulated Performance of PV Array Fed High Efficiency Induction Motor Drive for Water Pumping Using Boost Converter	165
4.8.1.1	Starting and Steady State Performance of Drive	165
4.8.1.2	Dynamic Performance of Proposed System During Step Decrease in Variable Irradiance	166
4.8.1.3	Dynamic Performance of Proposed System During Step Increase in Variable Irradiance	166
4.8.2	Experimental Performance of PV Array Fed High Efficiency Induction Motor Drive for Water Pumping Using Boost Converter	168
4.8.2.1	Test Results for MPPT	168
4.8.2.2	Performance of IMD: Starting and Steady State	168
4.8.2.3	Dynamic Performance: Step Change in Variable Irradiance	169
4.8.3	Simulated Performance of Single Stage PV Array Fed High Efficiency Induction Motor Drive for Water Pumping	170
4.8.3.1	Starting and Steady State Performance of Drive	170
4.8.3.2	Dynamic Performance of Proposed System During Change in Irradiance	172
4.8.3.2.1	Dynamic Performance of Proposed System During Step Decrease in Variable Irradiance	172
4.8.3.2.2	Dynamic Performance of Proposed System During Step Increase in Variable Irradiance	173
4.8.4	Experimental Performance of Single Stage Solar PV Fed High Efficiency Induction Motor Drive for Water Pumping	174
4.8.4.1	Test Results for MPPT	175
4.8.4.2	Performance of IMD: Starting and Steady State	175
4.8.4.3	Dynamic Performance of Drive: Decrease in Irradiance	177
4.8.4.4	Dynamic Performance of Drive: Increase in Irradiance	178

4.9	Economic Analysis of High Efficiency Induction Motor	179
4.9.1	Economic Analysis of the Usage of High Efficiency Induction Motor in Two Stage Solar PV Array Fed Water Pumping System	179
4.9.2	Economic Analysis of the Usage of High Efficiency Induction Motor in Single Stage Solar PV Array Fed Water Pumping System	180
4.10	Conclusion	181
CHAPTER V	UNIDIRECTIONAL POWER FLOW CONTROL BASED GRID INTERFACED SOLAR PV FED HIGH EFFICIENCY INDUCTION MOTOR DRIVE FOR WATER PUMPING	183-202
5.1	General	183
5.2	Configuration of Unidirectional Power Flow Control Based Grid Interfaced Two Stage Solar PV Fed Induction Motor Drive for Water Pumping	184
5.3	Design of Unidirectional Power Flow Control Based Grid Interfaced Two Stage Solar PV Fed Induction Motor Drive for Water Pumping	185
5.3.1	Design and Selection of Solar PV Array	186
5.3.2	Calculation of DC Link Voltage	186
5.3.3	Design of Common DC Link Capacitor	187
5.3.4	Design of VSI	187
5.3.5	Design of PFC Boost Converter for Single-Phase Grid System	187
5.3.6	Design of R-C Ripple Filter	188
5.4	Speed Estimation of Induction Motor Drive	189
5.5	Control of Unidirectional Power Flow Control Based Solar PV Fed Mechanical Sensorless Induction Motor Drive for Water Pumping	189
5.5.1	Perturb and Observe MPPT Algorithm	189
5.5.2	Power factor Correction of Single-Phase Grid	189
5.5.5	Field-Oriented Control of Induction Motor-Pump	190
5.6	MATLAB Based Modeling and Simulation of Unidirectional Power Flow Control Based Solar PV Fed Mechanical Sensorless Induction Motor Drive for Water Pumping	190
5.7	Hardware Implementation of Unidirectional Power Flow Control Based Solar PV Fed Mechanical Sensorless Induction Motor Drive for Water Pumping	190
5.8	Results and Discussion	192
5.8.1	Simulated Performance of Single-Phase Grid Interfaced Two Stage Solar PV Fed Mechanical Sensorless IMD Driven Water Pumping System with Unidirectional Power Flow Control	192
5.8.1.1	Starting and Steady State Performance of Drive	193

5.8.1.2	Dynamic Performance: Insolation Decrement (1000-200) W/m ²	193
5.8.1.3	Power Quality Performance of Utility Grid	194
5.8.2	Experimental Performance of Single-Phase Grid Interfaced Two Stage Solar PV Fed Mechanical Sensorless IMD Driven Water Pumping System with Unidirectional Power Flow Control	196
5.8.2.1	Test Results for MPPT	196
5.8.2.2	Starting Performance of the Drive	196
5.8.2.3	Steady State Performance of the Drive	198
5.8.2.4	Performance during Insolation Change	199
5.9	Economic Analysis of the Usage of High Efficiency Induction Motor	201
5.9.1	Economic Analysis of the Usage of High Efficiency Induction Motor in Unidirectional Power Flow Control Based Grid Interfaced Solar PV Array Fed Water Pumping System	202
5.11	Conclusions	202
CHAPTER VI	BIDIRECTIONAL GRID INTERFACED SOLAR PV FED HIGH EFFICIENCY INDUCTION MOTOR DRIVE FOR WATER PUMPING	203-228
6.1	General	203
6.2	Configuration of Grid Interactive Two Stage Solar PV Fed High Efficiency Induction Motor Drive for Water Pumping Based on Bidirectional Power Flow Control	204
6.3	Design of Two Stage Grid Interacted Solar PV Fed High Efficiency Induction Motor Drive for Water Pumping Based on Bidirectional Power Flow Control	205
6.3.1	Design and Selection of Solar PV Array	206
6.3.2	Design of Boost Converter	206
6.3.3	Design of DC link Capacitor	206
6.3.4	Design of DC link Voltage	206
6.3.5	Design of VSI	206
6.3.6	Design of Voltage Source Converter	207
6.3.7	Design of RC Ripple Filter	207
6.3.8	Design of Interfacing Inductor	208
6.3.9	Design of Water Pump	208
6.4	Speed Estimation of Induction Motor Drive	208
6.5	Control of Grid Interfaced Solar PV Fed Induction Motor Drive for Water Pumping Based on Bidirectional Power Flow Control	208
6.5.1	Perturb and Observe (P&O) Control Algorithm for MPPT	209

6.5.2	Bidirectional Power Flow Control Technique	209
6.5.3	PV Grid Integrated System with Field Oriented Control of IMD	209
6.6	MATLAB Based Modeling and Simulation of Two Stage Grid Interacted Solar PV Fed High Efficiency Induction Motor Drive for Water Pumping Based on Bidirectional Power Flow Control	209
6.7	Hardware Implementation of Two Stage Grid Interacted Solar PV Fed High Efficiency Induction Motor Drive for Water Pumping Based on Bidirectional Power Flow Control	211
6.8	Results and Discussion	211
6.8.1	Simulated Performance of the Two Stage Single Phase Grid Integrated PV array Fed System with Bidirectional Power Flow Control	212
6.8.1.1	Starting and Steady State Behavior of System	213
6.8.1.2	Dynamic Behavior of the System	214
6.8.2	Experimental Performance of the Two Stage Single Phase Grid Integrated PV array Fed System with Bidirectional Power Flow Control	216
6.8.2.1	Test Results for MPPT Efficiency	217
6.8.2.2	Starting and Steady State Performances of Proposed System	218
6.8.2.3	Dynamic Performances of PV Array-Grid Fed System	221
6.9	Economic Analysis of the Usage of High Efficiency Induction Motor	225
6.10	Conclusions	227
CHAPTER VII SINGLE PHASE GRID FED HIGH EFFICIENCY INDUCTION MOTOR DRIVE FOR FAN APPLICATION WITH POWER FACTOR CORRECTION		229-259
7.1	General	229
7.2	Configuration of Single-Phase Grid Fed High Efficiency Induction Motor Drive for Fan Application with Power Factor Correction	229
7.3	Design of Single-Phase Grid Fed High Efficiency Induction Motor Drive for Fan Application with Power Factor Correction	230
7.3.1	Calculation of DC Link Voltage	231
7.3.2	Design of Common DC Link Capacitor	231
7.3.3	Design of VSI	232
7.3.4	Design of PFC Boost Converter for Single-Phase Grid System	232
7.3.5	Design of R-C Ripple Filter	233
7.3.6	Design of Interfacing Inductor	234
7.3.7	Selection of IM	235
7.3.8	Design of fan	235
7.4	Speed Estimation of Induction Motor Drive	235

7.5	Control of Single-Phase Grid Fed High Efficiency Induction Motor Drive for Fan Application with Power Factor Correction	235
7.5.1	Power Flow Control of the Single-Phase Grid with Power Factor Correction	236
7.5.2	Field-Oriented Control of Induction Motor-Pump	238
7.6	MATLAB Based Modeling and Simulation of Single-Phase Grid Fed High Efficiency Induction Motor Drive for Fan Application with Power Factor Correction	239
7.7	Hardware Implementation of Single-Phase Grid Fed High Efficiency Induction Motor Drive for Fan Application with Power Factor Correction	239
7.8	Results and Discussion	240
7.8.1	Simulated Performance of Single-Phase Grid Fed High Efficiency Induction Motor Drive for Fan Application with Power Factor Correction	241
7.8.1.1	Starting and Steady State Performance of Drive	241
7.8.1.2	Dynamic Performance of the Drive	242
7.8.1.3	Power Quality Performance of Utility Grid	243
7.8.2	Experimental Performance of Single-Phase Grid Fed High Efficiency Induction Motor Drive for Fan Application with Power Factor Correction	243
7.8.2.1	Starting Response of the System	244
7.8.2.2	Steady State Performance of the System	246
7.8.2.3	Dynamic Performance during Grid Availability	247
7.8.2.4	Performance during Abnormal Grid Conditions	250
7.8.2.5	Harmonic Spectra Analysis of the Grid	252
7.9	Economic Analysis of the Usage of High Efficiency Induction Motor	258
7.10	Conclusions	258
CHAPTER VIII HIGH EFFICIENCY INDUCTION MOTOR DRIVE FOR SMALL COMMERCIAL ELECTRICAL VEHICLE		260-274
8.1	General	260
8.2	Configuration of High Efficiency Induction Motor Drive for Small Commercial Electrical Vehicle	260
8.3	Transmission System of Electric Vehicle	261
8.4	Design of High Efficiency Induction Motor Drive for Small Commercial Electrical Vehicle	262
8.4.1	Selection of DC Link Voltage	263
8.4.2	Design of Common DC Link Capacitor	263
8.4.3	Design of VSI	263
8.4.4	Design of Induction Motor	264

8.5	Speed Estimation of Induction Motor Drive	264
8.6	Control of High Efficiency Induction Motor Drive for Small Commercial Electrical Vehicle	264
8.7	MATLAB Based Modeling and Simulation of High Efficiency Induction Motor Drive for Small Commercial Electrical Vehicle	265
8.8	Hardware Implementation of High Efficiency Induction Motor Drive for Small Commercial Electrical Vehicle	266
8.9	Results and Discussion	266
	8.9.1 Single Stage Battery Fed High Efficiency Induction Motor Drive System	266
	8.9.1.1 Experimental Performance of Single Stage Battery Fed High Efficiency Induction Motor Drive System	266
	8.9.1.1.1 No Load Response of the System	267
	8.9.1.1.2 Load Response of the System	270
8.10	Conclusions	273
CHAPTER IX MAIN CONCLUSIONS AND SUGGESTIONS FOR FURTHER WORK		275-280
9.1	General	275
9.2	Main Conclusions	276
9.3	Suggestions for Further Work	278
REFERENCES		281-309
APPENDICES		310-316
LIST OF PUBLICATIONS		317-317
BIODATA		318-318

LIST OF FIGURES

- Fig. 3.1 Design algorithm for developing optimized high efficiency induction motor
- Fig. 3.2 Design procedure for conventional and pump application induction motor
- Fig. 3.3 Design procedure for conventional and electric vehicle application induction motor
- Fig. 3.4 Components of Initiation step
- Fig. 3.5 Single parameter performance effect on 0.75kW 4-pole IM (a) efficiency versus stator diameter (b) efficiency versus air-gap length (c) efficiency versus core length of stator
- Fig. 3.6 Single parameter performance effect on 0.75kW 4-pole IM (a)Copper loss Versus Output power (b) Core loss Versus Output power
- Fig. 3.7 Variables and Their Effect on the Efficiency of 0.75kW 4-pole IM
- Fig. 3.8 Components of Design Calculation Step
- Fig. 3.9 Winding diagram (a) conventional motor (b) improved efficiency ALRT
- Fig. 3.10 Components of design for squirrel cage rotor
- Fig. 3.11 Rotor slot geometry of 0.75kW 4pole three-phase induction motor (a) conventional IM (b) Optimized design IM(ALRT) (c) Optimized design IM(CuRT)
- Fig. 3.12 Reference slot design for rotor (a) conventional IM (b) Optimized design IM
- Fig. 3.13 Sequence of calculation of different components of electrical and magnetic loading
- Fig. 3.14 Sequence of calculation for short-circuit parameters
- Fig. 3.15 Sequence of calculation for performance parameters
- Fig. 3.16 Flow chart for the particle swarm optimization (PSO) algorithm
- Fig. 3.17 Flow chart of the Quasi-Newton Algorithm
- Fig. 3.18 Flow chart for the genetic algorithm
- Fig. 3.19 Slot design of stator and rotor of induction motor (a-b) conventional motor (c-d) improved efficient motor
- Fig. 3.20 Magnetic flux lines of the stator and rotor of 0.75kW 4pole induction motor (a) conventional IM (b) high efficiency IM(ALRT) (c) high efficiency IM(CuRT)
- Fig. 3.21 Magnetic flux lines of the stator and rotor of 1.5kW 4pole induction motor (a) conventional IM (b) high efficiency IM(ALRT) (c) high efficiency IM(CuRT)
- Fig. 3.22 Magnetic flux lines of the stator and rotor of 2.2 kW 4pole induction motor (a) conventional IM (b) high efficiency IM(ALRT) (c) high efficiency IM(CuRT)
- Fig. 3.23 Prototype performance type test setup for induction motor
- Fig. 3.24 Cooling curve for developed 2.2kW 4-pole three-phase induction motor with Aluminium as rotor bar material (ALRT)
- Fig. 3.25 Cooling curve for developed 1.5kW 4-pole three-phase induction motor with Aluminium as rotor bar material (ALRT)

- Fig. 3.26 Cooling curve for developed 0.75kW 4-pole three-phase induction motor with Aluminium as rotor bar material (ALRT)
- Fig. 3.27 Cooling curve for developed 2.2kW 4-pole three-phase induction motor with Copper as rotor bar material (CuRT)
- Fig. 3.28 Cooling curve for developed 1.5kW 4-pole three-phase induction motor with Copper as rotor bar material (CuRT)
- Fig. 3.29 Cooling curve for developed 0.75kW 4-pole three-phase induction motor with Copper as rotor bar material (CuRT)
- Fig. 3.30 No-load curve for 2.2kW 4-pole three-phase induction motor (ALRT)
- Fig. 3.31 No-load curve for 1.5kW 4-pole three-phase induction motor (ALRT)
- Fig. 3.32 No-load curve for 0.75kW 4-pole three-phase induction motor (ALRT)
- Fig. 3.33 No-load curve for 2.2kW 4-pole three-phase induction motor (CuRT)
- Fig. 3.34 No-load curve for 1.5kW 4-pole three-phase induction motor (CuRT)
- Fig. 3.35 No-load curve for 0.75kW 4-pole three-phase induction motor (CuRT)
- Fig. 3.36 Load curve between additional load losses and output torque of the developed 2.2kW 230V three-phase induction motor (ALRT) ap per the IEC60034-1:2017
- Fig. 3.37 Load curve between additional load losses and output torque of the developed 1.5kW 220V three-phase induction motor (ALRT) ap per the IEC60034-1:2017
- Fig. 3.38 Load curve between additional load losses and output torque of the developed 0.75kW 230V three-phase induction motor (ALRT) ap per the IEC60034-1:2017
- Fig. 3.39 Load curve between additional load losses and output torque of the developed 2.2kW 230V three-phase induction motor (CuRT) ap per the IEC60034-1:2017
- Fig. 3.40 Load curve between additional load losses and output torque of the developed 1.5kW 220V three-phase induction motor (CuRT) ap per the IEC60034-1:2017
- Fig. 3.41 Load curve between additional load losses and output torque of the developed 0.75kW 230V three-phase induction motor (CuRT) ap per the IEC60034-1:2017
- Fig. 3.42 Locked rotor curve 2.2kW 4P 230V three-phase induction motor ALRT
- Fig. 3.43 Locked rotor curve 1.5kW 4P 220V three-phase induction motor ALRT
- Fig. 3.44 Locked rotor curve 0.75kW 4P 230V three-phase induction motor ALRT
- Fig. 3.45 Locked rotor curve 2.2kW 4P 230V three-phase induction motor CuRT
- Fig. 3.46 Locked rotor curve 1.5kW 4P 220V three-phase induction motor CuRT
- Fig. 3.47 Locked rotor curve 0.75kW 4P 230V three-phase induction motor CuRT
- Fig. 3.48 (a-c) Ansys-RMxpvt efficiency versus speed curve for 0.75kW 4-pole 230V three-phase induction motor (a) conventional IM (b) proposed IM(ALRT) (c) proposed IM(CuRT)
- Fig. 3.49 (a-c) Ansys-RMxpvt efficiency versus speed curve for 1.5kW 4-pole 220V three phase induction motor (a) conventional IM (b) proposed IM(ALRT) (c) proposed IM(CuRT)
- Fig. 3.50 (a-c) Ansys-RMxpvt efficiency versus speed curve for 2.2kW 4-pole 230V three-phase induction motor (a) conventional IM (b) proposed IM(ALRT) (c) proposed IM(CuRT)

- Fig. 3.51 (a-c) Phase current versus speed for 0.75kW 4-pole three phase induction motor (a) conventional design IM (b) proposed high efficiency IM(ALRT) (c) proposed high efficiency IM(CuRT)
- Fig. 3.52 (a-c) Phase current versus speed for 1.5kW 4-pole three phase induction motor (a) conventional design IM (b) proposed high efficiency IM(ALRT) (c) proposed high efficiency IM(CuRT)
- Fig. 3.53 (a-c) Phase current versus speed for 2.2kW 4-pole three phase induction motor (a) conventional design IM (b) proposed high efficiency IM(ALRT) (c) proposed high efficiency IM(CuRT)
- Fig. 4.1 Block diagram of proposed two-stage field-oriented controlled induction motor drive
- Fig. 4.2 Block diagram of single stage solar PV array fed speed sensorless induction motor driven water pumping
- Fig. 4.3 Schematic of field-oriented control of induction motor drive for water pumping system
- Fig. 4.4 Schematic of PV array fed induction motor drive configuration for single-stage standalone water pumping system
- Fig. 4.5 (a-b) MPPT Control: Flowchart of perturb and observe algorithm (a) Double Stage (b) Single Stage
- Fig. 4.6 (a-b) Reference speed generation (a) ω_l estimation (b) feed-forward speed component
- Fig. 4.7 Field-oriented control of IMD
- Fig. 4.8 (a-c) MATLAB/Simulink model of solar PV fed induction motor drive for two stage solar PV array fed water pumping system (a) complete system (b) P&O MPPT algorithm (c) FOC for speed control
- Fig. 4.9 (a-c) MATLAB/Simulink model of solar PV fed induction motor drive for single stage solar PV array fed water pumping system (a) complete system (b) P&O MPPT algorithm (c) FOC for speed control
- Fig. 4.10 Photograph of Experimental prototype of the developed system
- Fig. 4.11 (a-b) Signal conditioning circuit for voltage sensors (a) schematic diagram (b) photograph of voltage sensor board
- Fig. 4.12 (a-b) Signal conditioning circuit for current sensors (a) schematic diagram (b) photograph of current sensor board
- Fig. 4.13 (a-b) Isolation and amplification circuit for gate drivers (a) schematic diagram (b) photograph of opto-isolation and amplification board
- Fig. 4.14 (a-b) Architecture of dSPACE 1202 (a) execution of control algorithm (b) CLP 1202
- Fig. 4.15 (a-b) Starting and Steady state response (a) PV array (b) induction motor-pump assembly
- Fig. 4.16 (a-b) Dynamic response of insolation decrease (1000-500) W/m² (a) solar PV array (b) induction motor-pump assembly
- Fig. 4.17 (a-b) Dynamic response of insolation change (500-1000) W/m² (a) solar PV array (b) induction motor-pump assembly
- Fig. 4.18 (a-b) MPPT efficiency at insolation level of (a) 1000 W/m² (b) 500 W/m²
- Fig. 4.19 Starting performance at insolation level of (a) 1000 W/m² (b) 500 W/m²

- (a-b)
- Fig. 4.20 Performance of IMD during steady state at insolation level of (a)1000 W/m² (b) 500 W/m²
- (a-b)
- Fig. 4.21 Performance indices during insolation change: 1000 W/m² to 500 W/m² to 1000 W/m²
- Fig. 4.22 Starting and MPPT at 1000 W/m² (a) PV array (b) Proposed Induction motor drive
- (a-b)
- Fig. 4.23 PV array dynamic performance during decrease in insolation from 1000 W/m² to 500 W/m² (a) PV array (b) IMD
- (a-b)
- Fig. 4.24 System performance on increasing insolation from 500 W/m² to 1000 W/m² (a) PV array (b) IMD
- (a-b)
- Fig. 4.25 MPPT of PV array at insolation of 1000 W/m²
- Fig. 4.26 Soft starting at 1000 W/m² irradiance (a) performance of the proposed system (b) Intermediate speed signal
- (a-b)
- Fig. 4.27 Soft starting at 500 W/m² irradiance (a) performance of the proposed system (b) Intermediate speed signal
- (a-b)
- Fig. 4.28 Steady state performance (a) 1000 W/m² (b) 500 W/m²
- (a-b)
- Fig. 4.29 Performance indices of (a) proposed system (b) waveforms showing sensed speed (ω_{sen}) and estimated speed (ω_m), during decrease in irradiance
- (a-b)
- Fig. 4.30 Performance indices of (a) proposed system (b) waveforms showing sensed speed (ω_{sen}) and estimated speed (ω_m), during increase in irradiance
- (a-b)
- Fig. 5.1 Single-phase unidirectional grid-solar PV interfaced system feeding FOC of induction motor drive
- Fig. 5.2 Unidirectional power flow control for single phase grid system
- Fig. 5.3 MATLAB/Simulink model (a) complete system (b) PWM control for PFC boost converter (c) reference current generator
- (a-c)
- Fig. 5.4 Block diagram of signal conditioning and control architecture of test setup
- Fig. 5.5 Starting and steady state performance of system fed by PV array (a) PV array and grid indices (b) motor indices
- (a-b)
- Fig. 5.6 Steady state performance of system fed by grid (a) PV array and grid indices (b) motor indices
- (a-b)
- Fig. 5.7 System performance during insolation change from 1000 W/m² to 200 W/m² (a)PV array-grid indices (b) induction motor drive indices
- (a-b)
- Fig. 5.8 System performance during insolation change from 200 W/m² to 1000 W/m² (a)PV array-grid indices (b) induction motor drive indices
- (a-b)
- Fig. 5.9 Grid performance (a) PFC of supply current and voltage (b) THD and harmonic spectrum of supply current i_g
- (a-b)
- Fig. 5.10 Experimental data for MPPT efficiency: (a) 1000 W/m² (b) 500 W/m²
- (a-b)
- Fig. 5.11 Starting performance of solar water pumping system when (a) Solar insolation is 1000W/m² and grid is available (b) Solar insolation is 0 W/m² and grid is available (c) Solar insolation is 1000W/m² and grid is not available
- (a-c)
- Fig. 5.12 Steady state performance when (a) Pump is running at rated speed (b) Grid alone is feeding the pump
- (a-b)

- Fig. 5.13 (a-b) Dynamic performance of solar water pumping system during grid connected operation when (a) Solar insolation changes from 1000W/m^2 to 500W/m^2 , (b) Solar insolation changes from 500W/m^2 to 1000W/m^2
- Fig. 5.14 (a-d) Harmonic spectrum (a) grid voltage v_g and grid current i_g at 1000 W/m^2 insolation (b) grid power drawn by the motor-pump system at 1000 W/m^2 insolation (c) grid voltage THD (d) grid current THD
- Fig. 5.15 (a-d) Harmonic spectrum (a) grid voltage v_g and grid current i_g at 500 W/m^2 insolation (b) grid power drawn by the motor-pump system at 500 W/m^2 insolation (c) grid voltage THD (d) grid current THD
- Fig.6.1 Block diagram of two stage single phase grid integrated solar PV fed high efficiency induction motor drive for water pumping system based on bidirectional power flow control.
- Fig.6.2 Block diagram of PLL based unit vector template generation
- Fig.6.3 (a-c) MATLAB/Simulink model of proposed system (a) overall system (b) single-phase grid (c) bidirectional power flow control
- Fig.6.4 (a-b) Hardware implementation (a) control block diagram (b) hardware setup
- Fig.6.5 (a-b) Starting response for solar PV array fed system (a) IMD (b) PV array and utility grid
- Fig.6.6 Harmonic spectra of grid current when system operated by utility grid only
- Fig.6.7 (a-b) Step decrement in insolation ($1000-200\text{ W/m}^2$) (a) IMD indices (b) PV array and utility grid indices
- Fig.6.8 (a-b) Step increment in insolation ($200-1000\text{ W/m}^2$) (a) IMD indices (b) PV array and utility grid indices
- Fig.6.9 (a-b) Condition pertaining changeover from PV array feeding pump to PV array feeding grid (a) IMD indices (b) PV array and utility grid indices
- Fig.6.10 Harmonic analysis of the supply when PV array feeding the grid.
- Fig.6.11 (a-b) MPPT efficiency curve of PV array (a) 500 W/m^2 (b) 1000 W/m^2
- Fig.6.12 (a-b) Starting performance of the system at (a) 1000 W/m^2 (b) 500 W/m^2
- Fig.6.13 Steady state performance of the system at 1000 W/m^2
- Fig.6.14 (a-b) Steady state performance of the system fed by utility grid only (a) grid, PV array and motor-pump indices (b) grid and motor-pump indices
- Fig.6.15 Steady state performance of the system fed when PV array is feeding the grid
- Fig.6.16 (a-b) System behavior operated by PV array-grid system during insolation change (a) ($1000-500\text{ W/m}^2$) (b) ($500-1000\text{ W/m}^2$)
- Fig.6.17 Dynamic performance during condition for changeover from PV array feeding utility grid to PV array feeding induction motor-pump set
- Fig.6.18 (a-b) Performance indices during dynamic condition: (a) PV array alone feeding pump to utility grid alone feeding pump (b) Utility grid alone feeding pump to PV array alone feeding pump
- Fig.6.19 (a-p) Total harmonic distortions and power factor of utility current (i_g) when (a-d) utility grid feeding the pump and no PV power is available i.e. the water pump fed by utility grid alone (e-h) PV array feeds power to grid and no pumping is

required (i-l) utility grid feeding the pump and no PV power is available (m-p) utility grid is fed by PV array at solar irradiation of 500W/m² and no pumping is required.

- Fig. 7.1 Configuration of single-phase grid fed fan type load profile system (IMD) with Power Factor Correction
- Fig. 7.2 Structure of the grid power flow control
- Fig. 7.3 Structure of SOGI
- Fig. 7.4 MATLAB/Simulink model of single-phase grid fed high efficiency induction motor driven fan load application system with Power Factor Correction
- Fig. 7.5 Developed hardware prototype of single-phase grid fed high efficiency induction motor driven fan load application system with power factor correction.
- Fig. 7.6 Performance of the PFC drive under speed control at 220-V ac input. (a) Starting performance, steady state of the proposed drive at 150 rad/sec. and dynamic performance when speed changes from 150 rad/sec to 100 rad/sec and then to 50 rad/sec. (b) Starting performance, steady state of the proposed drive at 50 rad/sec. and dynamic performance when speed changes from 50 rad/sec to 100 rad/sec and then to 150 rad/sec.
- Fig. 7.7 Grid performance (a) PFC of supply current and voltage (b) THD and harmonic spectrum of supply current i_g at 150rad/sec of fan speed (c) THD and harmonic spectrum of supply current i_g at 100rad/sec of fan speed
- Fig. 7.8 Starting performance of induction motor fan load drive in term of indices grid voltage (v_g), grid current (i_g), motor phase current (i_a) and induction motor fan speed (ω_m) when (a) Fan is started at low speed mode selection i.e.52 rad/sec. (b) Fan is started at medium speed mode selection i.e.105 rad/sec. (c) Fan is started at high speed mode selection i.e.157 rad/sec.
- Fig. 7.9 Steady state performance when IMFL is running at (a-b) Low speed i.e. 52 rad/sec (c-d) Medium speed i.e. 105 rad/sec (e-f) High speed i.e. 157 rad/sec
- Fig. 7.10 Dynamic Response of IMDFLA (a-b) Acceleration mode, Fan Speed Changing from Low to Medium to High (c-d) Deceleration mode, Fan Speed Changing from High to Medium to Low
- Fig. 7.11 Dynamic performance of fan type load system during grid connected operation during (a) Fast acceleration (Low-Medium-High) to fast deceleration (High-Medium-Low) (d) Fast deceleration (High-Medium-Low) to fast acceleration (Low-Medium-High)
- Fig. 7.12 Performance of IMD during (a) Grid voltage sag (b) Restoration
- Fig. 7.13 Performance of IMD during (a) Grid voltage swell (b) Restoration.
- Fig. 7.14 Performance of IMD during Grid Voltage Distortion (a) at high speed (b) at medium speed (c) at low speed
- Fig. 7.15 Harmonic spectrum for grid voltage v_g and grid current i_g at normal grid conditions (a-d) at fan speed of 157 rad/sec (e-h) at fan speed of 105 rad/sec (i-l) at fan speed of 52 rad/sec

- Fig. 7.16 (a-l) Harmonic spectrum for grid voltage v_g and grid current i_g while grid voltage sag (a-d) at fan speed of 157 rad/sec (e-h) at fan speed of 105 rad/sec (i-l) at fan speed of 52 rad/sec
- Fig. 7.17 (a-l) Harmonic spectrum for grid voltage v_g and grid current i_g while grid voltage swell (a-d) at fan speed of 157 rad/sec (e-h) at fan speed of 105 rad/sec (i-l) at fan speed of 52 rad/sec
- Fig. 7.18 (a-l) Harmonic spectrum for grid voltage v_g and grid current i_g while grid voltage is distorted (a-d) at fan speed of 157 rad/sec (e-h) at fan speed of 105 rad/sec (i-l) at fan speed of 52 rad/sec
- Fig.8.1 Schematic of overall system for single stage high efficiency induction motor drive for small commercial electric vehicle
- Fig.8.2 Basic Configuration of transmission system for small commercial EV
- Fig.8.3 MATLAB/Simulink model of induction motor driven electrical vehicle
- Fig.8.4 (a-c) Starting and steady state performance of system at reduced speed and no-load condition (a) Starting and Steady state performance in terms of $(V_{dc}, T_e, \omega_m, i_a)$ (b) Starting and Steady state performance in terms of $(i_\alpha, i_\beta, \omega_m, i_{bat})$ (c) intermediate signals during steady state in terms of $(i_\alpha, i_\beta, \psi_s, i_{bat})$
- Fig.8.5 (a-d) Reversal of speed at no-load condition in term of indices $(V_{dc}, T_e, \omega_m, i_a)$ (a) From -900 rpm to 0 rpm to 900 rpm (b) From -900 rpm to 0 rpm to 900 rpm (c) From 900 rpm to 0 rpm to -900 rpm to 0 rpm to 900 rpm (d) Step increase in speed from 100 rpm to 600 rpm to 900 rpm.
- Fig.8.6 (a-b) Regeneration phenomena while braking the electrical vehicle (a) change of speed from 900 rpm to 100 rpm and again to 900rpm, expressed in terms of $(i_\alpha, i_\beta, \omega_m, i_{bat})$ (b) change of speed from 900 rpm to 100 rpm and again to 600rpm expressed in terms of $(i_\alpha, i_\beta, \psi_s, i_{bat})$
- Fig.8.7 Performance of the system when the load torque is decreased and speed is maintained constant in term of indices $(V_{dc}, T_e, \omega_m, i_a)$.
- Fig.8.8 (a-c) Starting and steady state performance of the system at reduced speed and part load condition (a) Performance in terms of $(T_e, P_m, \omega_m, i_{bat})$ (b) Performance in terms of $(i_a, i_b, i_c, \omega_m)$ (c) intermediate signals in terms of $(\psi_\alpha, \psi_\beta, \omega_m, i_a)$
- Fig.8.9 (a-d) Performance of the system when the load torque is changed and speed is maintained constant in term of indices $(V_{dc}, T_e, \omega_m, i_a)$ (a) Increase in torque (b) Decrease in torque (c) Momentarily increase in torque and then decrease in torque (d) Momentarily decrease then increase in torque
- Fig.8.10 (a-d) Performance of the system when the load torque is changed and speed is maintained constant in term of indices $(T_e, P_m, \omega_m, i_a)$ (a) increase in speed (b) decrease in speed (c) step increase in speed (d) step decrease in speed

LIST OF TABLES

Table 2.1	Timeline of development of electric motor
Table 2.2	Technological Advancement in Solar Power Generation
Table 3.1	Conventional loss reduction measures in three phase induction motor
Table 3.2	Specifications of Conventional and Improved Designed for 0.75kW 4-pole 3-phase Induction Motor
Table 3.3	Specifications of Conventional and Improved Designed for 1.5kW 4-pole 3-phase Induction Motor
Table 3.4	Specifications of Conventional and Improved Designed for 2.2 kW 4-pole 3-phase Induction Motor
Table 3.5	Design Constraints for Performance Parameters for 0.75kW 4-pole 3-phase Induction Motor
Table 3.6	Parameter Constraints of Slot Geometry for 0.75kW 4-pole 3-phase Induction Motor
Table 3.7	Specification of Electrical Steel
Table 3.8	Loss Comparison for both grades of steel sheets for 0.75kW 4-pole induction motor
Table 3.9	Design Optimization Variables with their domain for a 0.75kW 4-pole 3-phase Induction Motor
Table 3.10	Design Matrix Generated by the 2^{6-2} fractional factorial Design Optimization Variables with their domain for a 0.75kW 4-pole 3-phase Induction Motor
Table 3.11	Box generators for the factorial design 2^{6-2}
Table 3.12	Contrast and Contribution for the factorial design 2^{6-2}
Table 3.13	Calculations of main dimensions for 0.75kW 4-pole 3-phase induction motor
Table 3.14	Selection of Current Density
Table 3.15	Winding Design Specifications of 0.75kW 4-pole induction motor
Table 3.16	Winding Design Specifications of 1.5kW 4-pole induction motor
Table 3.17	Winding Design Specifications of 2.2 kW 4-pole induction motor
Table 3.18	Selection of number of rotor slots
Table 3.19	Selection of Air-gap Length
Table 3.20	Comparison of different optimization algorithm for designing of a 0.75kW 4-pole three phase induction motor
Table 3.21	Optimized single-objective and multi-objective analysis of 0.75kW 4-pole three phase induction motor by using DOE/PSO combined approach
Table 3.22	Optimized slot design of 0.75kW 4-pole three phase induction motor by using DOE/PSO combined approach
Table 3.23	Optimized slot design of 1.5kW 4-pole three phase induction motor by using DOE/PSO combined approach
Table 3.24	Optimized slot design of 2.2kW 4-pole three phase induction motor by using DOE/PSO combined approach

Table 3.25	Comparison of calculations of total ampere turns for 0.75kW 4-pole induction motor
Table 3.26	Comparison of calculations for flux-density for 0.75kW 4-pole induction motor
Table 3.27	Comparison of calculations of total ampere turns for 1.5kW 4-pole 220V three-phase induction motor
Table 3.28	Comparison of calculations of total flux-density for 1.5kW 4-pole 220V three-phase induction motor
Table 3.29	Comparison of calculations of total ampere turns for 2.2kW 4-pole induction motor
Table 3.30	Comparison of calculations of total flux-density for 2.2kW 4-pole induction motor
Table 3.31	Terminal resistance of the stator winding of the developed three-phase induction motors at ambient temperature (Cold Resistance)
Table 3.32	Terminal resistance of the developed 2.2kW, 1.5kW and 0.75kW three-phase induction motor after heat-run test (Hot Resistance)
Table 3.33	Temperature-rise of the developed 2.2kW, 1.5kW and 0.75kW three-phase induction motor (ALRT) as per resistance method described in the IEC60034-1:2017
Table 3.34	Parameter monitored during the temperature-rise test of the developed 2.2kW 230V three-phase induction motor (ALRT) ap per the IEC60034-1:2017 (reading after every 30 minutes)
Table 3.35	Parameter monitored during the temperature-rise test of the developed 1.5kW 220V three-phase induction motor (ALRT) ap per the IEC60034-1:2017 (reading after every 30 minutes)
Table 3.36	Parameter monitored during the temperature-rise test of the developed 0.75kW 230V three-phase induction motor (ALRT) ap per the IEC60034-1:2017 (reading after every 30 minutes)
Table 3.37	Parameter monitored during the temperature-rise test of the developed 2.2kW 230V three-phase induction motor (CuRT) ap per the IEC60034-1:2017 (reading after every 30 minutes)
Table 3.38	Parameter monitored during the temperature-rise test of the developed 1.5kW 220V three-phase induction motor (CuRT) ap per the IEC60034-1:2017 (reading after every 30 minutes)
Table 3.39	Parameter monitored during the temperature-rise test of the developed 0.75kW 230V three-phase induction motor (CuRT) ap per the IEC60034-1:2017 (reading after every 30 minutes)
Table 3.40	No-load test performed at different voltage levels of the developed 2.2kW 230V three-phase induction motor (ALRT) ap per the IEC60034-1:2017.
Table 3.41	Calculations of the friction-windage loss and core-loss of the developed 2.2kW 230V three-phase induction motor (ALRT) ap per the IEC60034-1:2017
Table 3.42	No-load test performed at different voltage levels of the developed 1.5kW 220V three-phase induction motor (ALRT) ap per the IEC60034-1:2017
Table 3.43	Calculations of the friction-windage loss and core-loss of the developed 1.5kW 230V three-phase induction motor (ALRT) ap per the IEC60034-1:2017
Table 3.44	No-load test performed at different voltage levels of the developed 0.75kW 230V three-phase induction motor (ALRT) ap per the IEC60034-1:2017

Table 3.45	Calculations of the friction-windage loss and core-loss of the developed 0.75kW 230V three-phase induction motor (ALRT) ap per the IEC60034-1:2017
Table 3.46	No-load test performed at different voltage levels of the developed 2.2kW 230V three-phase induction motor (CuRT) ap per the IEC60034-1:2017
Table 3.47	Calculations of the friction-windage loss and core-loss of the developed 2.2kW 230V three-phase induction motor (CuRT) ap per the IEC60034-1:2017
Table 3.48	No-load test performed at different voltage levels of the developed 1.5kW 220V three-phase induction motor (CuRT) ap per the IEC60034-1:2017
Table 3.49	Calculations of the friction-windage loss and core-loss of the developed 1.5kW 220V three-phase induction motor (CuRT) ap per the IEC60034-1:2017
Table 3.50	No-load test performed at different voltage levels of the developed 0.75kW 230V three-phase induction motor (CuRT) ap per the IEC60034-1:2017
Table 3.51	Calculations of the friction-windage loss and core-loss of the developed 0.75kW 230V three-phase induction motor (CuRT) ap per the IEC60034-1:2017
Table 3.52	Calculations of the loss components of the developed 2.2kW 230V three-phase induction motor (ALRT) ap per the IEC60034-1:2017
Table 3.53	Load curve at different loads of the developed 2.2kW 230V three-phase induction motor (ALRT) ap per the IEC60034-1:2017
Table 3.54	Calculations of the loss components of the developed 1.5kW 220V three-phase induction motor (ALRT) ap per the IEC60034-1:2017
Table 3.55	Load curve at different loads of the developed 1.5kW 220V three-phase induction motor (ALRT) ap per the IEC60034-1:2017
Table 3.56	Calculations of the loss components of the developed 0.75kW 230V three-phase induction motor (ALRT) ap per the IEC60034-1:2017
Table 3.57	Load curve at different loads of the developed 0.75kW 230V three-phase induction motor (ALRT) ap per the IEC60034-1:2017
Table 3.58	Calculations of the loss components of the developed 2.2kW 230V three-phase induction motor (CuRT) ap per the IEC60034-1:2017
Table 3.59	Load curve at different loads of the developed 2.2kW 230V three-phase induction motor (CuRT) ap per the IEC60034-1:2017
Table 3.60	Calculations of the loss components of the developed 1.5kW 220V three-phase induction motor (CuRT) ap per the IEC60034-1:2017
Table 3.61	Load curve at different loads of the developed 1.5kW 220V three-phase induction motor (CuRT) ap per the IEC60034-1:2017
Table 3.62	Calculations of the loss components of the developed 0.75kW 230V three-phase induction motor (CuRT) ap per the IEC60034-1:2017
Table 3.63	Load curve at different loads of the developed 0.75kW 230V three-phase induction motor (CuRT) ap per the IEC60034-1:2017
Table 3.64	Lock rotor test measured for developed 2.2kW 230V three-phase induction motor (ALRT)
Table 3.65	Lock rotor test measured for developed 1.5kW 4-Pole three-phase induction motor (ALRT)
Table 3.66	Lock rotor test measured for developed 0.75kW 4-Pole three-phase induction motor (ALRT)

Table 3.67	Lock rotor test measured for developed 2.2kW 4-Pole three-phase induction motor (CuRT)
Table 3.68	Lock rotor test measured for developed 1.5kW 4-Pole three-phase induction motor (CuRT)
Table 3.69	Lock rotor test measured for developed 0.75kW 4-Pole three-phase induction motor (CuRT)
Table 3.70	Starting Current measured for developed high efficiency three-phase induction motor
Table 3.71	Starting Torque measured for developed high efficiency three-phase induction motor
Table 3.72	Comparative data for loss component of 0.75kW 4-pole three-phase induction motor
Table 3.73	Comparative data for loss component of 1.5 kW 4-pole induction motor
Table 3.74	Comparative data for loss component of 2.2 kW 4-pole induction motor
Table 3.75	Comparative starting performance data
Table 4.1	PV Array design (Simulation Data)
Table 4.2	PV Module (Simulation Data)
Table 4.3	Calculation for Boost Converter
Table 4.4	Calculation for DC Link Capacitor
Table 4.5	Calculation of DC Link Voltage
Table 4.6	Calculation of VA rating of VSI
Table 4.7	PV Array Design for Single Stage System (Simulation Data)
Table 4.8	PV Module (Simulation Data)
Table 4.9	Calculation for DC Link Capacitor
Table 4.10	Calculation of DC Link Voltage
Table 4.11	Calculation of payback of incremental investment for improved design motor
Table 4.12	Calculation of direct saving in costs by using improved design motor and hardware in two stage standalone PV array fed water pumping system
Table 4.13	Calculation of direct saving in costs by using improved design motor and hardware in single stage standalone PV array fed water pumping system
Table 5.1	Calculation of payback of incremental investment for improved design motor
Table 5.2	Calculation of direct saving in costs by using improved design motor and hardware in unidirectional grid interfaced solar PV array fed water pumping system
Table 6.1	Calculation of payback of incremental investment for improved design motor
Table 6.2	Calculation of direct saving in costs by using improved design motor and hardware in bidirectional grid interfaced solar PV array fed water pumping system
Table 7.1	Calculation of DC Link Voltage
Table 7.2	Calculation of DC Link Capacitor

Table 7.3	Calculation of VSI
Table 7.4	Power quality performance of the utility grid
Table 7.5	Calculation of payback of incremental investment for improved design motor
Table 8.1	Calculation of DC Link Capacitor
Table 8.2	Calculations for VSI Rating

LIST OF ABBREVIATIONS

EEC	Electrical Equivalent Circuit
MEC	Magnetic Equivalent Circuit
FEM	Finite Element Method
GA	Genetic Algorithm
PSO	Particle Swarm Optimization
QNA	Quasi Newton Algorithm
DOE	Design of Experiments
CAD	Computer Aided Design
ALRT	Aluminium Rotor
CuRT	Copper Rotor
AT	Ampere Turns
PV	Photovoltaic
EV	Electric Vehicle
PMSM	Permanent Magnet Synchronous Motor
DC	Direct Current
BLDC	Brushless DC
MPPT	Maximum Power Point Tracking
VSI	Voltage Source Inverter
PQ	Power Quality
THD	Total Harmonics Distortion
IEEE	Institute of Electrical and Electronics Engineers
PD	Positive Displacement
SVM	Space Vector Modulation
VSC	Voltage Source Converter
PFC	Power Factor Correction
MNRE	Ministry of New and Renewable Energy
BIS	Bureau of Indian Standards
IEC	International Electrotechnical Commission
CEC	Clean Energy Council
IM	Induction Motor
PMSM	Permanent Magnet Synchronous Motor
SRM	Switched Reluctance Motor

SyRM	Synchronous Reluctance Motor
P&O	Perturb and Observe
CSC	Canonical Switching Cell
MRAS	Model Reference Adaptive System
EMF	Electromotive Force
PI	Proportional Integral
FOC	Field-Oriented Control
AC	Alternating Current
BES	Battery Energy Support
IMD	Induction Motor Drive
IGBT	Insulated Gate Bipolar Transistor
DSP	Digital Signal Processor
DSO	Digital Signal Oscilloscope
CPU	Central Processing Unit
ADC	Analog to Digital Converter
DAC	Digital to Analog Converter
SPS	Sim Power System
DTC	Direct Torque Control
SOC	State of Charge
UVT	Unit Vector Template
STC	Standard Temperature and Pressure
LPF	Low Pass Filter
PLL	Phase-Locked Loop
DRAM	Dynamic Random-Access Memory
SOGI	Second Order Generalized Integral

LIST OF SYMBOLS

V_{mpp}, V_{mp}	Solar PV voltage (V) of one module and one array at MPP
I_{mpp}, I_{mp}	Solar PV current (A) of one module and one array at MPP
V_{oca}, V_{oc}	Open-circuit voltage (V) of one module and one array
I_{sca}, I_{sc}	Short-circuit current (A) of one module and one array
V_{pv}, I_{pv}	Solar PV array voltage (V) and current (A)
N_{ser}, N_{par}	Number of series and parallel modules
P_{mp}	Solar PV power of one array at MPP
D	Duty ratio
f_s	Switching frequency of boost inductor
T_{sw}	Time period of VSI
L_l	Boost inductor
ΔI_l	Ripple allowed in converter current
V_L, I_L	Boost inductor voltage (V), inductor current (A)
V_D, V_{sw}	Diode voltage, switch voltage in boost converter
C_{dc}	DC link capacitor
V_{dc}, V_{dc1}	DC link voltage, maximum ripple allowed in DC link voltage
I_{dc}	DC link current
a	Overloading factor
i_a	Motor phase current
V_p, V_{L-L}	Phase voltage, line voltage of induction motor
m	Modulation index
V_{VSI}, I_{VSI}	Voltage rating of VSI, current rating of VSI
K_V and K_I	Voltage safety factor, current safety factor
K_l	Pump constant
P_m	Rated power of induction motor
ω_{sl}, ω_e and ω_m	Slip speed, synchronous speed and motor speed in rad/s
ω_{ref}	Reference speed
v_a, v_b and v_c	Phase voltages (V) of induction motor
v_α, v_β	Voltages in α - β domain
i_α, i_β	Motor currents in α - β domain
$\Psi_\alpha, \Psi_\beta, \Psi_s$	Fluxes in α - β domain, resultant flux
$\Psi_{\alpha r}, \Psi_{\beta r}, \Psi_r$	Rotor fluxes in stationary reference frame, resultant flux
L_r, L_s, L_m	Rotor inductance, stator inductance and mutual inductance
L_{lr}, L_{ls}	Rotor leakage inductance, stator leakage inductance

R_r, R_s	Rotor resistance, stator resistance
V_{ref}	Reference voltage (V)
ψ_{ds}^*, ψ_{ds}	Reference d-axis flux (Wb), actual d-axis flux (Wb)
i_{ds}^*, i_{ds}	Reference d-axis current (A), actual d-axis current (A)
i_{qs}^*, i_{qs}	Reference q-axis current (A), actual q-axis current (A)
T_e^*, T_e	Reference developed torque (Nm), estimated developed torque (Nm)
P	Number of poles
T_p	Pump torque (Nm)
η	Efficiency (%)
V_{bat}	Battery voltage
ω_L	Fundamental frequency (rad/s)
f_{sw2}	Switching frequency of PFC boost converter
L_2	PFC boost inductor
Δi_{gL}	Ripple allowed in PFC boost inductor current
R_f, C_f	Resistance (Ω) and capacitance (μF) of RC filter
T_{sw2}	Switching time of PFC boost converter
v_g, i_g	Grid voltage (V), grid current (A) of single-phase utility grid
L_i	Interfacing inductor
W	Winding Pitch
τ_p	Pole Pitch measured as slot pitch
q_s	Slot per pole per phase
m	No of total phases
δ_s	Current Density for the stator windings (A/mm^2)